Available online at www.sciencedirect.com
ScienceDirect
Ceramics International 35 (2009) 3111–3116
CERAMICS INTERNATIONAL
www.elsevier.com/locate/ceramint

Structure and properties of short fibre reinforced silica matrix composite foams

Sarika Mishra [a], R. Mitra [b,*], M. Vijayakumar [a]

[a] Defence Metallurgical Research Laboratory, Kanchanbagh, Hyderabad 500 058, India
[b] Department of Metallurgical and Materials Engineering, Indian Institute of Technology, Kharagpur, West Bengal 721 302, India

Received 19 January 2009; received in revised form 27 March 2009; accepted 28 April 2009
Available online 7 June 2009

Abstract

Glass (GFC) and silica (SFC) fibre reinforced silica matrix composite foams with 84–90% porosity content have been developed through slurry-based processing, involving random dispersion of 10 wt.% fibres with aspect ratios of >1000 in hydrophobized silica-based suspensions, and direct foaming for air entrapment. Fibre entanglement has not been found either in the suspensions or in the sintered composite foams. Microstructural and mercury porosimetry studies of the composite foams have shown a trimodal size distribution with small (4–8 μm), medium (40–200 μm), and large (∼1 mm or more) pores. The pores appear spherical and interconnected, with the fibres embedded in cell-walls or struts. The dynamic Young's modulus of the silica-coated GFCs is found to be ∼3.5 and ∼5.2 times that of the coated and uncoated monolithic silica foams, respectively, confirming that both fibre-reinforcement and the presence of surface coating are beneficial for increase in stiffness of the composite foams.

Keywords: A. Sintering; B. Composites; B. Fibres; C. Mechanical properties; D. SiO_2

1. Introduction

Silica-based ceramics and composites are ideally suited for use in the thermal protection systems for the space shuttle and other re-entry type aerospace vehicles [1–6] in view of their low density, low thermal conductivity and acceptable levels of mechanical properties. Processing of multiphase ceramic composite foams with specified pore size distribution and relative density is challenging. The two major hurdles for the fabrication of ceramic composite foams are: (i) achieving a uniform dispersion of fibres, and (ii) foaming to obtain the desired pore size distribution.

Slurry-based processing has been developed as a potential route for incorporation of fibres in the matrix to produce short fibre reinforced ceramic composites [5–9]. Unlike dry powder processing, the slurry-based processing gives the opportunities for achieving a uniform distribution of various phases through co-dispersion in a solvent [10,11]. Furthermore, the "*direct foaming method*" [12–14] is one of the simplest ways of introducing pores in the ceramic foams. In this process, the foams are prepared by entrapment of air in the suspension by a controlled mechanical operation, and stabilization of the air bubbles, followed immediately by casting, drying and sintering of the foam [15]. The total porosity in such foams is proportional to the amount of air incorporated in the suspension during the foaming process. Little information exists on the application of direct foaming approach for fabrication of porous short fibre reinforced silica composites.

Earlier studies [16] have shown that achieving a uniform dispersion of fibres in a slurry becomes difficult, once the fibre content exceeds 5 wt.%, because of the natural tendency of fibres to entangle and agglomerate. However, in a recent study by Mishra et al. [17], it has been demonstrated that short fibres of either glass or quartz with aspect ratios up to 1000 and quantity of up to 10 wt.% can be uniformly dispersed through a novel dispersion method, which involves the addition of silica powder hydrophobized with cetyl trimethyl ammonium bromide (CTAB) maintaining a fibre to powder ratio (FPR) of 1:4. The present study is focused on examination of the structure, permeability and Young's modulus of the 10 wt.%

* Corresponding author. Tel.: +91 3222 283292; fax: +91 3222 282280.
E-mail address: rahul@metal.iitkgp.ernet.in (R. Mitra).

0272-8842/$36.00
doi:10.1016/j.ceramint.2009.04.027

silica or glass fibre reinforced composites, processed using the combination of fibre dispersion and direct foaming methods mentioned above.

2. Experimental procedure

The investigated glass and silica fibre reinforced composites will be referred to as GFC and SFC, respectively, in the following text.

2.1. Raw materials

Fused silica powder (Industrial grade, $d_{50} = 20$ μm) was used as a starting material. Commercially available E-glass and silica (quartz) fibres with 10 μm diameter were chopped into ∼20 mm long strands, and subsequently used for the present study.

2.2. Fibre processing

Both the chopped glass and quartz fibres were desized with 0.2 M dilute nitric acid solution, and soaked overnight in order to remove the amino ($-NH_2$) group from "*sizes*" in the form of soluble salts. The fibres were then repeatedly washed with distilled water and finally subjected to washing with acetone in order to dissolve the polymeric constituents of the *sizes*. The desized fibres were then dried in air at room temperature. After the completion of chopping and desizing operations, the glass or silica fibre strands were dispersed in water containing 0.05% CTAB solution as a dispersant by mechanical agitation for ∼8–10 h in small amounts such as ∼2 g per liter. Once the fibres were dispersed in a large excess of water, a small amount of fused silica powder hydrophobized with CTAB was added in FPR of 1:4 to the suspension, and mixed for 30 min to stabilize the dispersion. This dispersion was then left for 16 h to allow settling down of the suspended solids. The excess water was then decanted off. The dispersion of fibres and powders was subsequently added to silica slurry for further processing of the composite foams, as is described in the following section.

2.3. Fabrication of fibre reinforced composite foams

The fused silica powder ($d_{50} = 20$ μm, industrial grade) along with 5 wt.% Al_2O_3 and 0.05% CTAB (98% pure, S.D. Fine Chemicals Ltd.) was ball milled for 100 h using alumina balls as the milling media in 1:1 ratio, so as to have a "pre-treated" powder mixture with an average particle size of ∼5 μm. Subsequently, a slurry with solids loading of 25–35 vol.% was prepared in aqueous medium by mixing the pre-treated powder, a premix containing the binders and the suspension with dispersed fibres, by pot milling (30 rpm) of the constituents for 2 h, using alumina balls as the milling media. The binder solution (premix) for preparing the suspensions, comprised 4-vol.% poly-vinyl alcohol (PVA, mol. wt. 125,000 Fischer, LR grade), 10 wt.% sucrose and 5 vol.% of colloidal silica (40% SiO_2 content). Afterwards, the milled slurry was subjected to foaming for 3–4 h in order to entrain air into the suspension. The foaming operation involved *tumbling* or periodic changes in the orientation of the container by 90° for effective air entrapment. Furthermore, the foamed suspensions were allowed to age for a period of 10–15 min for stabilization and then cast into suitable rectangular moulds. The cast samples were dried initially under controlled conditions (Osworld humidity chamber, $T = 30$ °C, relative humidity = 40–80%) in a graded fashion, and then in a hot air oven up to 100 °C. Finally the fully dried composite green bodies were subjected to binder burn out and sintering at 1100 °C using a heating rate of 1 °C/min. A coating of silica slurry was applied to some of the GFC foam green bodies for the purpose of surface densification [15], in order to close the larger pores at and near the surfaces.

2.4. Characterization of composite foams

The density (ρ) of the composite foams prepared through the method described in Section 2.3 was calculated by measuring the specimen mass and volume. The theoretical density (ρ_s) of the composite was calculated by applying the rule of mixtures to the volume fractions of the constituents. The relative densities (ρ/ρ_s) of the composite foams were obtained by normalizing the bulk density with the theoretical density of the material. The microstructures of the sintered foam samples were studied using an optical microscope and a scanning electron microscope (SEM) model Leo 440i (Carl Zeiss, Jena, Germany). The optical microscope was equipped with a Biovis MV500 image acquisition and analysis software (Bio Vismat Plus, Version 1.5), which was used for analysis of pore size distribution. The pore size distribution and surface area of the sintered cylindrical samples with 9.25 mm diameter and 18 mm height was estimated by mercury intrusion porosimetry on a Quantachrome Poremaster version 4.01 (Boynton Beach, Florida). The contact angle of mercury with the foam surface was 140° during the study. The room temperature air permeability of the sintered disks was determined by measuring the pressure drop across the sample as a function of the gas flow rate, following the procedure described in a previous publication [15].

The dynamic Young's moduli of the surface-coated GFC samples with dimensions of 10 mm × 10 mm × 70 mm were measured using a Dynamic Elastic Properties Analyzer (Jagdish Electronics, Bangalore, India), by using an impulse excitation technique. For determination of the Young's modulus, the specimens were subjected to vibration mechanically with the help of a tapping device, and the signal generated was analyzed using fast Fourier transform by considering the natural frequency of vibration, following the procedure suggested in ASTM C1259-01 [18]. Dynamic Young's moduli of the coated and uncoated, monolithic silica foams were also measured using a similar method for the purpose of comparison with those of the GFCs.

3. Results and discussion

One of the major achievements of this work is that porous composite panels with dimensions of 100 mm × 100 mm × 25 mm, with randomly dispersed short fibres accounting

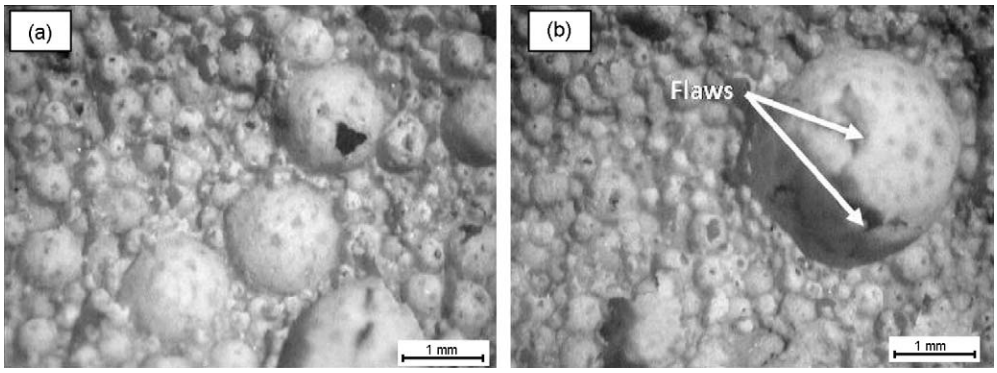

Fig. 1. Optical micrographs of the SFC foams showing: (a) open and interconnected porosity; and (b) flaws in the walls of a larger pore.

Table 1
Typical absolute and relative densities of GFC and SFC foams in green and sintered condition.

Sample	Absolute density (g cm^{-3})	Relative density (%)
GFC (green)	0.345	15.8
GFC (sintered)	0.349	16.0
SFC (green)	0.298	13.7
SFC (sintered)	0.266	12.2

for 10 wt.%, and porosity content of ∼88 vol.%, could be fabricated successfully after optimization of several process variables.

3.1. Density and shrinkage

Visual inspection of the green bodies of porous composites has shown no evidence of cracking, in spite of the linear shrinkage of 4% recorded upon drying up to 100 °C. Table 1 shows the absolute and relative densities of the green bodies and sintered foams of the GFCs and SFCs, each with 10 wt.% fibre reinforcement. The minor difference between the green and sintered densities of the composite foams indicates that the shrinkage on sintering is small, as the pore structure and size distribution present in the green bodies is mostly retained.

3.2. Microstructure

The study of microstructure includes primarily the characterization of pore structure and pore size distribution, as well as the silica coating on the surface of the foam.

3.2.1. Optical microscopy and image analysis

Typical optical micrographs depicting the pore structure of the SFC foams are shown in Fig. 1(a) and (b). Examination of several such micrographs leads to the following inferences: (i) the microstructure contains both open and interconnected porosity; (ii) there is an apparent bimodal distribution of pore sizes with the average size of the smaller and larger pores being $\leq$200 μm and $\geq$1 mm, respectively; and (iii) the overall average pore count is 10–12 pores per inch (ppi). While the average size of the large pores is ∼1 mm in the optical micrograph shown in Fig. 1(a), a pore with diameter of ∼2.6 mm is shown in Fig. 1(b). The formation of interconnections between the pores (Fig. 1) is attributed to rupture of the thinner partition walls between the cells.

An optical micrograph depicting the cross-section of surface-coated GFC green body is shown in Fig. 2. The average thickness of the surface coating has been found to be ∼250 μm. From a close examination of the pore structure along the cross-section of the GFC, it is clear that the pore size is much finer inside the coating than that found below it inside the foam sample. From the results of image analysis, the sizes of pores inside the surface coating have been found to be in the range of 30–50 μm.

3.2.2. Scanning electron microscopy: pore morphology and distribution of fibres

The microstructures of the SFC foams are shown at different magnifications in the SEM images, presented in Fig. 3(a)–(e). On examination of the microstructures shown in Fig. 3, it is obvious that: (i) the pores are spherical, open and interconnected [Fig. 3(a)–(d)]; (ii) the average cell wall thickness is ∼10–20 μm [Fig. 3(b)]; (iii) the fibres are randomly distributed and appear embedded either in the struts or in the cell walls

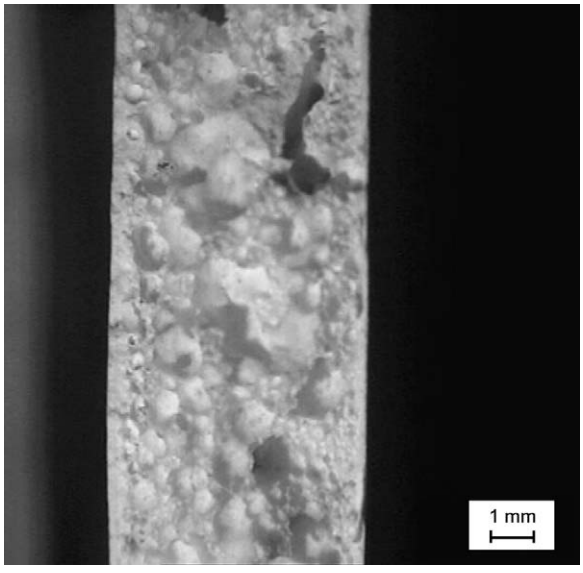

Fig. 2. Optical micrograph depicting the cross-section of the GFC foam with a surface coating of ∼250 μm thickness.

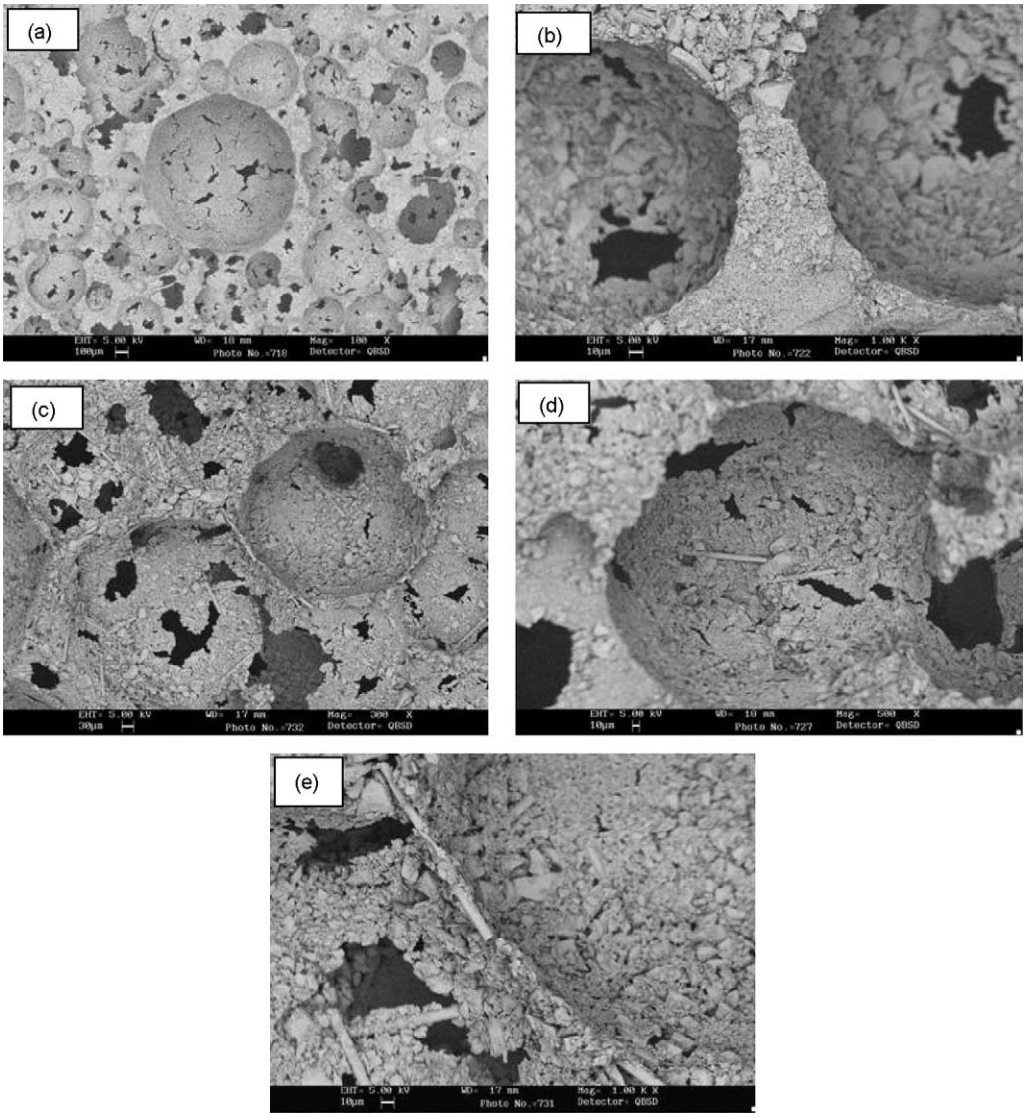

Fig. 3. SEM micrographs of the SFC foams showing: (a) the pore morphology at low magnification, (b) a single strut (partition wall) showing strut thickness at higher magnification, (c) random fibre distribution (low magnification), (d) random fibre distribution within a bubble depression, (e) fibre distribution within the strut along with flaws at higher magnification.

[Fig. 3(c)–(e)]; and (iv) the average fibre length appears to be not more than ∼200 μm [Fig. 3(c)–(e)]. This suggests that the average fibre length has been significantly reduced from the initial length of 20 mm due to breakage during processing. A close inspection of the microstructures [Fig. 3(c)–(e)] also leads to the inference that the fibres in the struts are surrounded by large pores with irregular shapes. Some of the fibres appear non-uniform in diameter along their length because of twists, as shown in Fig. 3(e).

3.3. Mercury porosimetry: pore size distribution and surface area

The results of mercury porosimetry are shown in Fig. 4. From the histogram depicting the normalized pore volume per unit mass in the SFC foam for different pore diameters, as shown in Fig. 4(a), it is obvious that (i) the pore size distribution is bimodal, with both small (4–8 μm) and large (40–200 μm) pores; and (ii) the pore volume of the smaller pores peaks at 6 μm, while the maximum pore volume for the larger size range is observed for pores having 70 μm diameter. Thus, comparison of the results of mercury porosimetry with the pore sizes determined from the optical microscopy studies is suggestive of three different size-ranges: (i) small (4–8 μm), (ii) medium (40–200 μm), and (iii) large (∼1 mm) or more. While the small pores (4–8 μm) are not resolved in the optical microscope images [Fig. 1(a) and (b)], the large pores (∼1 mm) are hardly detectable through the present mercury porosimetry studies. This is because the pressure of the mercury in the finer pores is much higher compared to that in the larger pores, making the measurements less sensitive for the larger pores (∼1 mm or larger).

The plot of cumulative surface area (CSA) per unit mass of the foam against the pore diameter, as shown in Fig. 4(b),

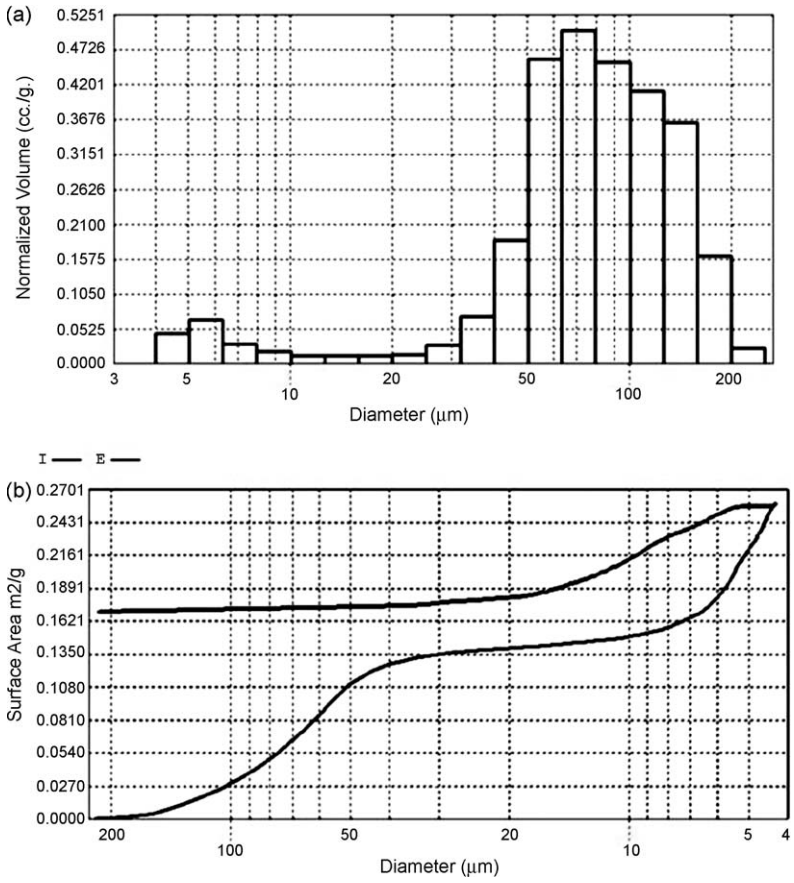

Fig. 4. The results of mercury porosimetry carried out on samples of SFC: (a) histogram of normalized volume fraction as a function of pore size distribution; (b) plot showing the CSA as a function of pore diameter (measured through mercury porosimetry).

indicates that: (i) the CSA decreases with increasing pore size; (ii) the CSA per unit mass corresponding to the mean pore sizes of 6 and 70 μm are 0.18 and 0.06 m^2/g, respectively, (iii) the cumulative CSA per unit mass of the foam is found as 0.257 m^2/g, and (iv) the CSA per unit mass corresponding to the extruded volume of mercury is higher than that of the intruded volume by 0.162 m^2/g. The large difference (0.162 m^2/g) between the CSAs per unit mass for the intruded and extruded volumes of mercury in Fig. 4(b) is probably due to the presence of smaller pores within the bigger pores inside the SFC foams. These smaller pores within the bigger pores are responsible for entrapment of mercury and there is little driving force for bringing the mercury out of the pores during the extrusion phase.

3.4. Permeability

The permeability of the SFC with 88 vol.% porosity content has been found as 5.6×10^{-10} m^2. Comparison of permeability of the SFC with that of the monolithic silica foams [15] having a similar value of relative density indicates that the permeability of latter is higher by 2 orders of magnitude. The lower permeability observed in the porous SFC than in the monolithic silica foams is attributed to the presence of fibres, interrupting the pore interconnections in the former material.

3.5. Young's modulus

Bar charts representing the dynamic Young's moduli of the surface-densified (coated) GFC foams are shown against the relative densities in Fig. 5. In addition, bar charts representing the dynamic Young's moduli of both the coated and uncoated

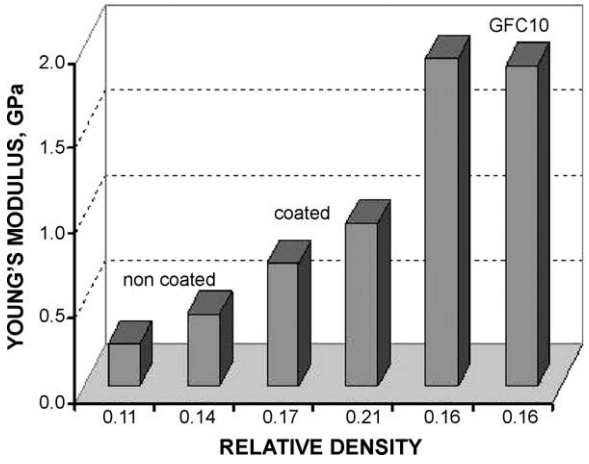

Fig. 5. Bar charts depicting the elastic moduli of the coated GFC with 10 wt.% fibre (marked as GFC10) along with those of the coated and non-coated silica foams (marked as "coated" and "non-coated").

monolithic silica foams (without fibre reinforcements) are included in Fig. 5 for a comparative analysis to determine the effects of both the fibre reinforcement and the surface densification. Comparison of the bar charts in Fig. 5 reveals that the coating on monolithic silica foams causes a ∼1.5-fold increase in the Young's modulus over that of uncoated foams, for nearly similar relative densities. Furthermore, comparison of the bar charts in Fig. 5 also leads to the inference that the presence of glass fibre reinforcements is solely responsible for the fact that Young's moduli of the GFC foams are ∼3.5 times that observed for the coated silica foams with similar relative densities. Thus, on the basis of the results of the present study, it may be inferred that the use of glass fibres as reinforcements significantly enhances the stiffness of the foams, when surface coating is applied. The increase in dynamic Young's modulus on application of surface coatings on the silica foams is attributed primarily to decrease in the surface flaw size. Since much higher strains are caused at and near the surface than near the centre by the mechanically induced vibrations of the bar type samples, it is intuitive that reduction in size and density of surface flaws by densification with application of coating is significantly beneficial for the dynamic Young's modulus of both the monolithic and composite foams.

4. Conclusions

Composite foams reinforced with random dispersion of either glass or silica (quartz) fibres with aspect ratios ≥1000 and accounting for 10 wt.%, have been developed. A uniform dispersion of fibres without any entanglement could be obtained in a suspension containing an appropriate mix of hydrophobized silica and binders. Furthermore, direct foaming method has been optimized for the preparation of SFC and GFC foams with specified relative densities, as well as with desirable combinations of pore morphology and size distribution. Relatively large porous silica-based composite panels with dimensions of 100 mm × 100 mm × 25 mm, having randomly dispersed short fibres of glass or silica accounting for 10 wt.%, and porosity content of ∼88 vol.%, could be fabricated successfully after optimization of the process parameters.

The pore size distribution in the composite foams appears to be trimodal with the small (4–8 μm), medium (40–200 μm) and large (≥1 mm) pores. The microstructure of the porous composites shows spherical and interconnected cells with fibres, embedded either in the cell-walls or in the tortuous struts. The GFC foams with surface coating shows a ∼3.5-fold enhancement in the dynamic Young's modulus with respect to that of coated silica foams of similar relative density, implying that the presence of fibre reinforcements in the composite foams leads to enhancement in their stiffness. Furthermore, comparison of the dynamic Young's moduli of the uncoated and coated monolithic silica foams shows ∼1.5-fold increment caused by the reduction in the size and density of surface flaws due to the application of silica coating. The results of this study show that the slurry composition, direct foaming method and surface densification can be optimized to tailor silica matrix composite foams with desirable combinations of relative density, pore size distribution and mechanical properties.

Acknowledgements

The authors are thankful to Director, Defence Metallurgical Research Laboratory, Hyderabad for his encouragement and support. One of the authors (S.M.) is thankful to the Defence Research and Development Organization, New Delhi for the financial support during the work.

References

[1] H.W. Rauch Sr., W.H. Sutton, L.R. McCrieght, Refractory Materials: A Series of Monographs, vol. 3, Ceramic Fibers and Fibrous Composite Materials, Academic Press, New York, 1968.
[2] L.J. Korb, C.A. Morant, R.M. Calland, C.S. Thatcher, The shuttle orbiter thermal protection system, Ceram. Bull. 60 (11) (1981) 1188–1193.
[3] D.B. Leiser, M. Smith, H.E. Goldstein, Developments in fibrous refractory composite insulation, Ceram. Bull. 60 (11) (1981) 1201–1204.
[4] K.J. Korb, H.M. Claney, The shuttle orbiter thermal protection system: a material and structural overview, in: Proceedings of the 26th National SAMPE Symposium, Los Angeles, USA, (1981), pp. 232–249.
[5] D.C. Jia, Y. Zhou, Effect of fiber content on properties of a short carbon fiber reinforced fused silica matrix composite, J. Adv. Mater. 38 (3) (2006) 21–26.
[6] F.P. Meyer, G.D. Quinn, J.C. Walck, Reinforcing fused silica with high purity fibers, Ceram. Eng. Sci. Proc. 6 (7–8) (1985) 646–656.
[7] E. Fitzer, R. Gadow, Fiber reinforced composites via sol–gel route, in: R.E. Tressler, G.L. Messing, C.G. Pantano, R.E. Newham (Eds.), Tailoring of Multiphase and Composite Ceramics, Plenum Press, New York, USA, 1986, pp. 571–607.
[8] M. Schmucker, B. Kanka, H. Schneider, Temperature-induced fibre/matrix interactions in porous alumino-silicate ceramic matrix composites, J. Eur. Ceram. Soc. 20 (14–15) (2000) 2491–2497.
[9] R.W. Rice, Mechanisms of toughening in ceramic matrix composites, Ceram. Eng. Sci. Proc. 2 (7–8) (1981) 661–701.
[10] J.A. Lewis, Colloidal processing of ceramics, J. Am. Ceram. Soc. 83 (10) (2000) 2341–2359.
[11] F.F. Lange, Powder processing science and technology for increased reliability, J. Am. Ceram. Soc. 72 (1) (1989) 3–15.
[12] J.S. Woyansky, C.E. Scott, W.P. Minnear, Processing of porous ceramics, Am. Ceram. Soc. Bull. 71 (11) (1992) 1674–1682.
[13] P. Sepulveda, Gelcasting foams for porous ceramics, Am. Ceram. Soc. Bull. 76 (10) (1997) 61–65.
[14] A.R. Studart, U.T. Gonzenbach, E. Tervoort, L.J. Gauckler, Processing routes to macroporous ceramics: a review, J. Am. Ceram. Soc. 89 (6) (2006) 1771–1789.
[15] S. Mishra, R. Mitra, M. Vijayakumar, Light weight silica tiles through foam casting method, J. Eur. Ceram. Soc. 28 (9) (2008) 1769–1776.
[16] J. Blome (Swiss Aluminium Limited), Molten metal filter. U.S. Patent 4 265 659, 5 May 1981.
[17] S. Mishra, R. Mitra, M. Vijayakumar, A novel route for the dispersion of fibers for the preparation of fiber reinforced porous composites, Mater. Lett. 62 (12–13) (2008) 2025–2028.
[18] ASTM Standard test method for dynamic Young's modulus, shear modulus and Poisson's ratio by impulse excitation of vibration, ASTM C 1259-01, Annual Book of ASTM Standards, American Society for Testing and Materials International, West Conshohocken, PA, USA, 2005.